

Large-scale Integration of Experimental and Computational Data for 2D Materials

Mohammad A. Akhound,¹ Tara M. Boland,¹ Mikkel O. Sauer,¹ Matthias Batzill,² Moses A. Bokinala,³ Stela Canulescu,⁴ Yury Gogotsi,³ Philip Hofmann,⁵ Andras Kis,⁶ Jiong Lu,⁷ Thomas Michely,⁸ Søren Raza,⁹ Wencai Ren,¹⁰ Joshua A. Robinson,¹¹ Zdenek Sofer,¹² Jing H. Teng,¹³ Søren Ulstrup,⁵ Meng Zhao,¹³ Xiaoxu Zhao,¹⁴ Jens J. Mortensen,¹ Thomas Olsen,¹ and Kristian S. Thygesen¹

¹*CAMD, Department of Physics, Technical University of Denmark, DK - 2800 Kongens Lyngby, Denmark**

²*Department of Physics, University of South Florida, Tampa, FL 33620, USA.*

³*Materials Science and Engineering Department and A. J. Drexel Nanomaterials Institute, Drexel University, 3141 Chestnut Street, Philadelphia, Pennsylvania 19104, United States*

⁴*Department of Electrical and Photonics Engineering, Technical University of Denmark, Roskilde 4000, Denmark*

⁵*Department of Physics and Astronomy, Aarhus University, 8000 Aarhus C, Denmark*

⁶*Institute of Electrical and Microengineering, cole Polytechnique Fdrale de Lausanne (EPFL), Lausanne, Switzerland*

⁷*Institute for Functional Intelligent Materials, National University of Singapore*

⁸*Physikalisches Institut, Universitt zu Kln, D-50937 Kln, Germany*

⁹*Department of Physics, Technical University of Denmark, DK - 2800 Kongens Lyngby, Denmark*

¹⁰*Shenyang National Laboratory for Materials Science, Institute of Metal Research, Chinese Academy of Sciences, 72 Wenhua Road, Shenyang 110016, P. R. China.*

¹¹*Materials Science and Engineering at the Pennsylvania State University, United States*

¹²*Department of Inorganic Chemistry, University of Chemistry and Technology Prague, Technick 5, 166 28 Prague 6, Czech Republic*

¹³*Institute of Materials Research and Engineering (IMRE), Agency for Science, Technology and Research (A*STAR), Singapore, 138634 Singapore*

¹⁴*School of Materials Science and Engineering, Peking University, Beijing 100871, China*

The past decade has seen rapid growth in the number of experimentally realized two-dimensional (2D) materials with diverse chemical and physical properties. However, information on their crystal structure, synthesis routes, and measured or predicted properties, remains scattered across thousands of publications. Here we consolidate this fragmented knowledge by establishing X2DB – an open infrastructure that integrates experimental and computational data on 2D materials. Using extensive literature mining and direct community uploads, we identify 370 unique 2D materials that have been realized in monolayer or few-layer form, and link them to their digital counterparts in computational databases, enabling consistent *ab initio* characterization of their properties across monolayer, bilayer and bulk forms. We describe the structure and content of the database highlighting its support for community uploads, illustrate how it can be used to generate new scientific insight and introduce a hierarchical classification of the known set of 2D materials. Our work provides a foundation for the integration and cross-fertilization of experimental and theoretical knowledge, opening new avenues for data-driven, predictive synthesis of novel 2D materials.

I. INTRODUCTION

Two-dimensional (2D) materials have emerged as a distinct class of materials with exceptional physical properties and broad technological potential[1] that spans from catalysis [2] and energy storage[3] to photonics [4], electronics [5], and quantum devices[6]. The reduced dimensionality simplifies the space of possible 2D materials compared to bulk solids – for example, there are only 80 layer groups versus 231 three-dimensional space groups[7]. Yet, the known 2D materials exhibit vast diversity in electronic behavior covering band insulators[8], Mott insulators[9], semiconductors[10], semi-metals[11], metals[12], superconductors[13], ferroelectrics[14], and various types of topological[15] and magnetic phases[16].

The high pace at which new 2D materials and related physical phenomena have been discovered, has made it difficult to organize the resulting knowledge efficiently. In contrast to bulk materials, where more than a century of research has been consolidated in handbooks and digital databases like the Inorganic Crystal Structure Database (ICSD)[17] and the Materials Project[18], experimental data on 2D materials remain scattered across thousands of publications. While several computational databases on 2D materials exist[19–21], no comparable resource exist for experimental realizations.

This lack of structured experimental data creates a critical gap: of the thousands of 2D materials predicted by computations[19, 22], only a small subset has been synthesized. This discrepancy arises from several factors. First, the synthesis process of 2D materials can be complex and require highly specific conditions[23] - both for bottom-up growth and for top-down exfoliation[24]. In addition, the experimental techniques used to syn-

* akhound@dtu.dk, thygesen@fysik.dtu.dk

synthesize and characterize 2D materials are still evolving and often involve advanced equipment that is not universally accessible[25]. Computational predictions, while valuable, are often based on simple descriptors that are easy to calculate but rely on assumptions that may not fully represent the real-world situation[26]. Most notably, the decomposition energy (aka the energy above the convex hull) is widely used as a descriptor for thermodynamic stability even though it neglects effects of temperature/entropy, substrate interactions, and chemical environments. Despite the common use of this and other simple descriptors (e.g. phonons for dynamical stability[27] and interlayer binding energy for exfoliability[22]), their importance for stability under realistic conditions and relation to synthesizability, remains unclear. We note in passing that more advanced stability descriptors have been proposed to predict e.g. chemical exfoliability[28] and environmental stability of 2D materials[29].

The gap between theoretically predicted materials and experimental realizations raises important questions regarding the relevance and predictive power of established computational materials-discovery approaches and underscores the challenges of synthesizing novel 2D materials. [30, 31] An essential first step towards answering these questions and overcoming the challenges, is to establish a systematic overview of the current landscape of experimentally realized 2D materials and connect them to relevant computations.

Earlier work in this direction has focused on known bulk compounds with potential for exfoliation. Following initial work by Lebegue *et al.*[32], several groups employed topological screening of experimental crystal structure databases in combination with DFT calculations, concluding that nearly 2000 known bulk phases can potentially be mechanically exfoliated.[22, 33, 34] More recently, Bjrk *et al.* used the formation of MXenes from MAX phases as a guiding example to computationally identify non-vdW layered compounds potentially exfoliable by selective etching.[28] However, aside from a few well known reference cases, these studies did not assess which materials have actually been realized in atomically thin form.

In this work, we provide the first systematic mapping of experimentally realized 2D materials and furthermore link them directly to their counterparts in open computational databases. By screening the 2D materials literature using a combination of filtering, ranking, and manual structure verification, we identify 270 unique materials that have been synthesized in few-layer form and whose chemical formula appears in the Computational 2D Materials Database (C2DB). To enable consistent descriptions, we introduce a unified taxonomy for 2D materials covering crystal structure, sample morphology, synthesis route, and characterization methods, and we curate this information in the open-access Experimental 2D Materials Database (X2DB). Via its full integration with computational monolayer, bilayer, and bulk databases, the X2DB allows seamless exploration of consistently cal-

culated properties across length scales (monolayer, bilayer, bulk) for experimentally relevant materials. Importantly, X2DB also supports community uploads, allowing that the database continues to expand and remains a living resource for the field. Indeed, community submissions have already expanded the X2DB catalogue by approximately 100 additional unique 2D materials.

II. EXPERIMENTALLY REALIZED 2D MATERIALS

The workflow used to identify experimentally realized 2D materials and connect them to monolayers in the C2DB is illustrated in Fig.1. The process began by filtering approximately 90 million scientific papers from the Web of Science Core Collection by selecting those whose abstracts contained keywords indicative of experimental studies on 2D materials (see green box in Fig.1). This initial filtering yielded around 200,000 papers; their distribution over publication years shown in Fig. 2. Next, we refined the selection by retaining only papers whose abstracts include a chemical formula matching a stable monolayer in the C2DB (here stable means an energy above the convex hull below 0.3 eV/atom). This filters out reports on materials that are unlikely to be found in the C2DB, and reduced the dataset to approximately 29,000 papers. We note that this filter induces a bias towards theoretically predicted materials with the risk of missing genuinely new (not theoretically explored) materials. On the other hand, it ensures that the experimental reports can be linked to relevant computational data, which is a key feature of our work.

The 29,000 papers were then ranked according to a set of relevance criteria, including citation count, publication year, and the presence of density functional theory (DFT) calculations supporting the experiments. Starting from the top-ranked papers, we performed manual inspection of each paper to verify that it indeed contains experimental synthesis and characterization of a 2D material in atomically thin form.

Following this manual verification, we identified 280 unique materials reported in 221 papers (some papers report multiple materials). For each material, we performed a detailed comparison of the reported experimental data with the structural polytypes of the relevant chemical formula available in the C2DB to verify the crystal structure. Since the reported experimental data do not always allow an unambiguous identification of the structure, we assign a *confidence level* to the pairing between an experimentally realized material and a C2DB monolayer structure, taking values 1 (low), 2 (medium), or 3 (high). Out of the 280 materials, 163 were assigned a confidence level of 3, indicating that their structural phase could be identified without ambiguity.

The literature mining described above was performed to populate the database with a diverse initial set of materials. As a second step, the database was opened up to

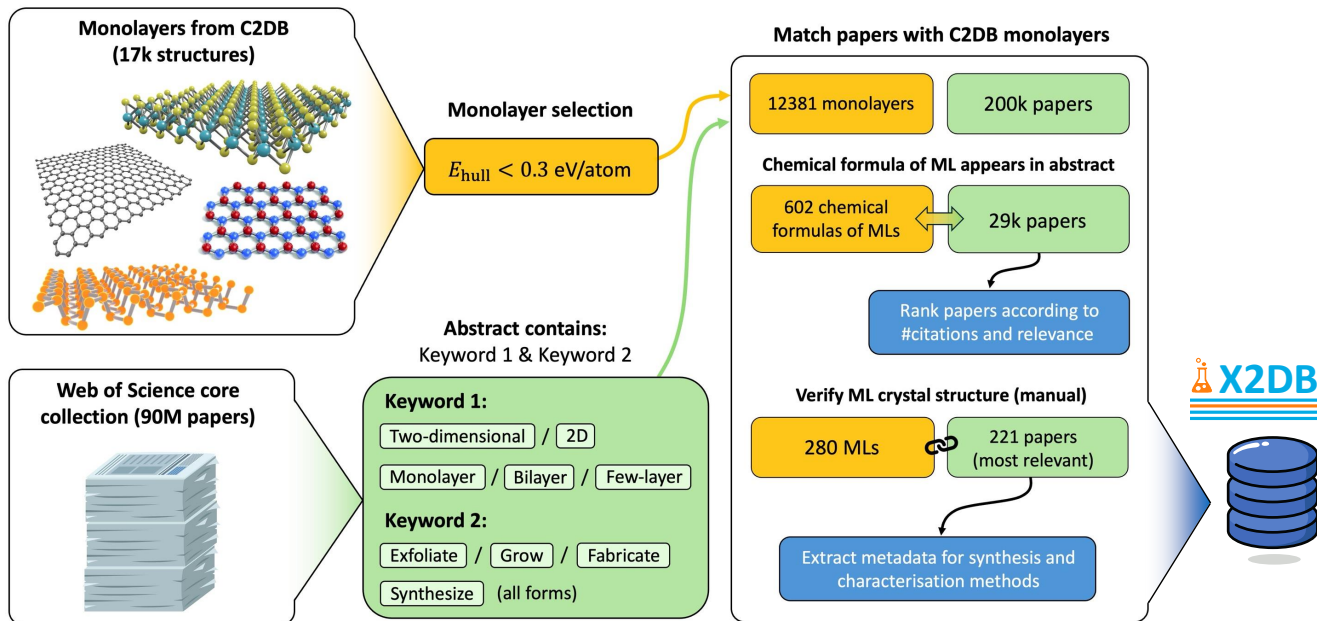


FIG. 1: **Workflow used to identify experimentally reported 2D materials and link them to C2DB.**

Relevant publications are identified by searching the abstract for specific keywords that indicate that the paper reports on the synthesis or exfoliation of a material in atomically thin form. The materials reported in the papers are linked to structures in the C2DB monolayer database using manual inspection of the crystal structure. Finally, the information describing the reported material and the employed synthesis and characterization methods, is extracted and classified according to the 2D materials taxonomy.

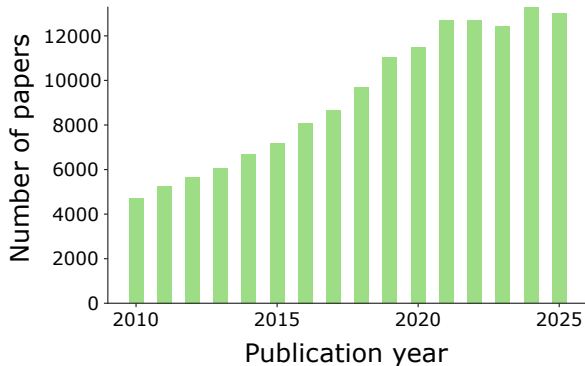


FIG. 2: Papers published on experimentally realized 2D materials since 2010. More precisely, the graph shows the 200k publications selected by the search criteria in the green box in Fig. 1, sorted according to publication year.

accept registrations of materials/publications from a limited group of experimental researchers who also provided feedback on the infrastructure design and user interface. At the time of writing, the X2DB holds 550 entries covering 370 unique chemical formulas of which 210 have been matched with a monolayer in C2DB with highest confidence level.

On this basis, we can conclude that at least 370 dis-

tinct materials have so far been experimentally realized in monolayer or few-layer form. This number should, for obvious reasons be considered as a lower bound. An overview of the materials (the subset identified after the initial literature mining step) is provided in the Supplementary Information (SI), along with references to the corresponding publications and a summary of the experimental methods used. Additionally, each material is linked to its monolayer in the C2DB, where a variety of computed properties are available. We note that this information, and more, is also available via the X2DB website.

III. THE 2D MATERIALS TAXONOMY

Experimental 2D materials science is a diverse, cross-disciplinary field that encompasses a wide range of synthesis and measurement techniques. To promote a coherent and consistent description of experimental 2D materials data, X2DB uses a high-level taxonomy specifically tailored to atomically thin samples. The taxonomy organizes information into conceptual categories covering crystal structure, sample morphology, synthesis, characterization methods, and measured properties, rather than individual measurement datasets. A schematic overview is provided in Figure 3.

The taxonomy's primary aim is to standardize the rep-

resentation of experimentally realized 2D materials and to establish a controlled vocabulary for their description. It can be seen as a compact parameterization of "what matters experimentally for 2D materials", designed to support statistical inference across the literature.

In addition to the main categories shown in Figure 3, it includes additional sub-categories and predefined labels, e.g. for the most common substrates, synthesis techniques, and characterization methods. A complete description of the taxonomy is provided in the SI. The selection of (sub)categories and labels used in the taxonomy, is based on the 221 publications analyzed at the final stage of the literature mining. While the predefined labels of the taxonomy are often sufficient to describe all relevant aspects of synthesized 2D materials, they are obviously not exhaustive; X2DB therefore also accommodates any user-specified text within the relevant categories. Below we provide an overview of the main categories of the taxonomy.

A. Structure and Composition

This category describes the pristine material using standard crystallographic terminology, including its chemical formula, structural phase, and crystal symmetries of the as-grown/as-exfoliated 2D sample. In addition to the conventional 3D space group, the taxonomy also includes the 2D crystal system describing the symmetry of the in-plane lattice (square, rectangular, hexagonal, oblique). This is particularly relevant for ultrathin materials for which the space group may be difficult to determine or not even well-defined due to limited out-of-plane periodicity. Certain classes of 2D materials, in particular MXenes, may contain unresolved mixed/non-stoichiometric surface termination groups (e.g. O, OH, F) resulting from the chemical synthesis. These termination groups can strongly influence the properties of the materials. It is possible to specify such termination groups alongside the chemical formula of the bare, unterminated 2D material. For 2D materials produced by exfoliation technique, the chemical formula and space group of the parent bulk material can be specified separately.

In addition to the symmetry and crystal phase, a number of *structural classifier* keywords can be used to describe the 2D material in greater detail. These include (but are not limited to) *vdW-layered material* and *non-vdW material*, *multiphase* (denoting samples containing distinct regions of different structural phases[35]), *defect-derived* (for crystal structures that are obtained from an ideal parent crystal by introducing defects such as vacancies[36]), *substrate-bonded* (referring to cases where the 2D material is chemically bonded to the substrate, such as silicene on Ag(111)[37]), *intercalated* and *self-intercalated* (for vdW structures with hetero or native atoms in the vdW gaps[38, 39]).

B. Sample Morphology

The qualitative material features are complemented by quantitative attributes that describe the sample morphology. These comprise the sample thickness (categorized as "<1 nm", "1-3 nm", "3-10 nm", ">10 nm"), the number of layers - or, for non-layered materials, the number of out-of-plane unit cells - and the lateral flake size. Thickness and lateral size refer to the thinnest samples obtained.

C. Synthesis Methods

Synthesis methods are classified into bottom-up growth and top-down exfoliation. The bottom-up category is further divided into bulk growth methods, which produce macroscopic crystals or powders for subsequent exfoliation, and direct 2D growth methods, which directly deposit or synthesize the material in atomically thin form. The top-down category encompasses the most widely used exfoliation techniques including dry and liquid-phase mechanical exfoliation, selective etching, and intercalation.

D. Substrates

Substrates play a crucial role for both the growth and properties of 2D materials. The taxonomy distinguishes between growth substrates, used for direct synthesis, e.g. chemical vapor deposition (CVD) or molecular beam epitaxy (MBE), and transfer substrates used for characterization and/or device integration. Use of metallic growth substrates often lead to strongly bonded, non-transferable 2D materials (in such cases, it may be more appropriate to use the term adsorption layer rather than a 2D material). In addition to the direct chemical interaction, the substrate also influences electronic properties of the 2D material via non-local dielectric effects, which modify the (screened) Coulomb interactions in the 2D material leading to renormalization of band structures, optical excitations, and transport properties[40–42]. Consequently, not only the chemical inertness and structural/electronic uniformity of the substrate is of importance, but also its dielectric properties.

E. Characterization Methods

The characterization methods included in the taxonomy cover the most widely used techniques in the field, including scanning and transmission electron microscopy, photoelectron spectroscopies, scanning probe techniques, X-ray absorption and diffraction methods, optical imaging and spectroscopy (including Raman and second harmonic generation), magnetic resonance techniques, and electrical measurements. A free-text field is available

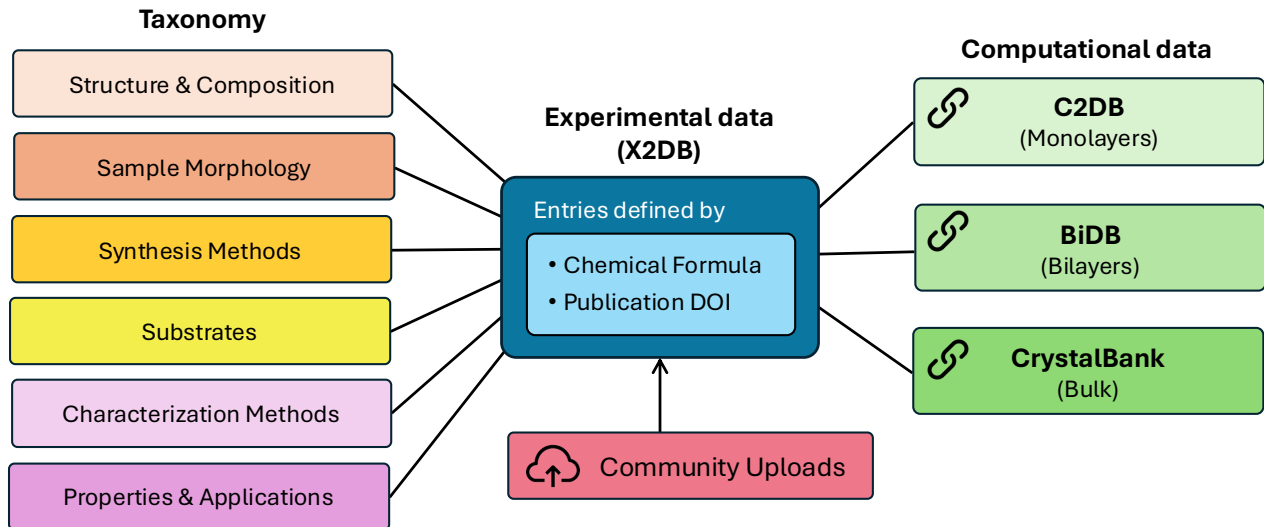


FIG. 3: **The Experimental 2D Materials Database.** The taxonomy (left) provides a controlled language for describing 2D materials. Colored boxes represent the taxonomy’s top-level categories each containing sub-categories and predefined labels as detailed in the SI. Experimental materials can be linked to corresponding structures in computational databases of monolayers, bilayers, and bulk solids. An associated confidence level (number between 1 and 3) is used to indicate the reliability of the link. New records - defined by the material (chemical formula) and a related publication DOI – can be registered by external users via a simple web form.

for providing more details and/or characterization techniques not covered by the pre-defined descriptors.

F. Properties and Applications

This category is used to describe the measured properties and/or explored applications reported in the associated publication. The taxonomy provides a set of predefined labels covering the most central topical areas in 2D materials research, such as linear and nonlinear optics, phase transitions, transport regimes, magnetic order, optoelectronics, spintronics, batteries, and (electro)catalysis. Although extensive, the list is not exhaustive and is intentionally kept relatively coarse-grained. A free-text field is available for more detailed descriptions, including properties or applications not covered by the predefined labels, as well as for reporting quantitative measurement data.

G. Linking to Computational Data

A key feature of X2DB, is its integration with computational databases. When uploading an entry, users may provide a unique identifier (UID) for a corresponding structure in the C2DB monolayer database and assign the match a confidence level from 1-3. Entries that are matched with a C2DB monolayer structure upon registration, will contain a link to the relevant monolayer in C2DB from its X2DB page. In addition, for matches

with high confidence level, links to the corresponding homobilayer structures (all stable stacking configurations) in the computational bilayer database, BiDB[43], will be generated automatically and inserted on the X2DB page. We note that the interlayer binding energies available in BiDB can be regarded as a proxy for the exfoliation energy – an approach justified by the fact that a bilayer’s binding energy is a well-approximated measure (within 10%) for the exfoliation energy of a thick slab.[44] Moreover, by comparing the electronic band structures of the monolayer and homobilayers one can get an idea of the strength and importance of interlayer hybridization upon stacking.

Similarly, entries that hold a space group for the bulk form of the 2D material, are automatically linked to the relevant bulk crystal structure in the computational database CrystalBank. This makes it possible to explore the detailed crystal structure and the electronic band structure of the bulk compound.

The C2DB, BiDB, and CrystalBank databases are internally consistent: All crystal structures and properties are computed using the same electronic structure code (GPAW[45]) and numerical settings. This uniformity allows direct comparison of properties – such as structural parameters, magnetic moments, and band gaps – across monolayers, bilayers, and bulk structures. Had the calculations been performed with different codes, methods, or parameter settings, any variations in the calculated properties could reflect numerical discrepancies rather than intrinsic physical differences.

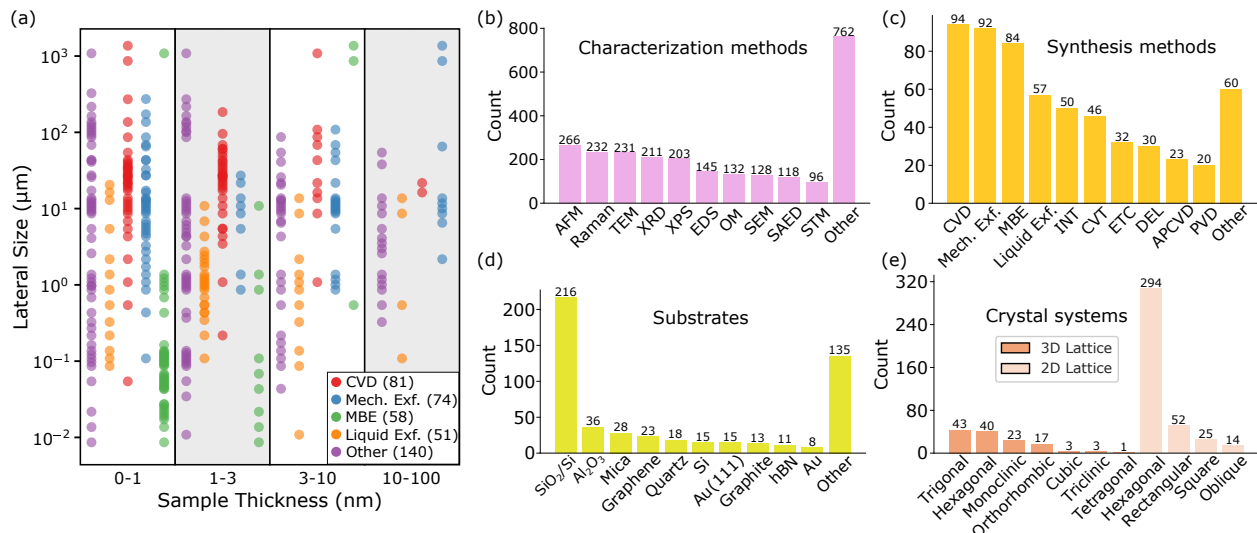


FIG. 4: **Statistical Overview of Selected Data from X2DB.** (a) Morphological parameters (lateral size and thickness) of experimentally realized 2D materials as a function of synthesis method. (b-e) Distributions of the most frequently reported characterization methods, synthesis methods, crystal systems (for both the 2D in-plane lattice and the 3D lattice), and substrates used for growth or transfer. Each plot highlights the top 10 most common reports, while all other, less frequent entries are grouped in a single combined bar to provide a comprehensive overview.

IV. THE DATABASE

X2DB organizes information in *entries*, each defined by the chemical formula of a material and the DOI of a publication reporting an experimental study of that material in few-layer form. The information contained in an entry is described using the 2D materials taxonomy introduced above. While the taxonomy covers both van der Waals layered crystals and compounds without a naturally layered topology, non-stoichiometric compounds, heterostructures, and twisted moiré structures are currently not supported.

New entries can be uploaded to X2DB by external users via a simple web form. The only requirement is that the user possesses an ORCID. In particular, they need not be an author of the associated publication. Because each entry represents a material-publication pair, multiple materials can be linked to the same publication, and multiple publications can be linked to the same material. Currently, most materials are associated with only a single or a few publications. However, a popular material like MoS₂, has been registered in more than 20 entries, each with a different publication. Such diversity in publication space is highly useful as it can provide an overview of different employed synthesis methods and resulting sample morphologies as well the range of property measurements and applications explored for a given 2D material.

As an example of the type of information available in X2DB, Fig. 4 presents some statistical overviews of selected data sets. Fig. 4(a) shows the lateral size versus thickness of 2D samples obtained by different syn-

thesis/exfoliation methods, where each point represents one of the 470 entries in X2DB. It can be seen that molecular beam epitaxy (MBE) typically produces thin (mostly monolayer) samples of small lateral dimensions ($< 1\mu\text{m}$). In contrast, chemical vapor deposition (CVD) yields samples with a broader thickness range and significantly larger lateral sizes ($10 - 100\mu\text{m}$). Dry mechanical exfoliation methods (e.g. Scotch tape/stamping) produce samples with thickness and lateral size distributions similar to those obtained by CVD, whereas liquid-phase exfoliation techniques (e.g., ultrasonication or high-shear methods) generally yield slightly thicker samples with smaller lateral sizes ($0.1 - 10\mu\text{m}$).

Figures 4(b-d) show the distributions of registered materials over characterization methods, synthesis routes, and substrates used for growth or transfer. In each case, the ten most frequent categories are shown explicitly, while the remainder are grouped under Others. While there is a clear predominance of SiO₂ substrates, no single synthesis or characterization method stands out as particularly dominant. Instead, the distributions are relatively flat with long tails (note the sizable Others category), highlighting the large diversity of techniques employed in the field. Panel (e) shows the distribution of crystal systems (for both the 2D in-plane lattice and the 3D lattice) of the registered 2D materials. There is a pronounced predominance of hexagonal crystal structures, consistent with the close-packed nature of most 2D materials. We note that there are fewer registrations of the 3D crystal symmetry. This is because determination of the 3D space group, or even just the 3D crystal system, requires samples of a certain thickness in order for the

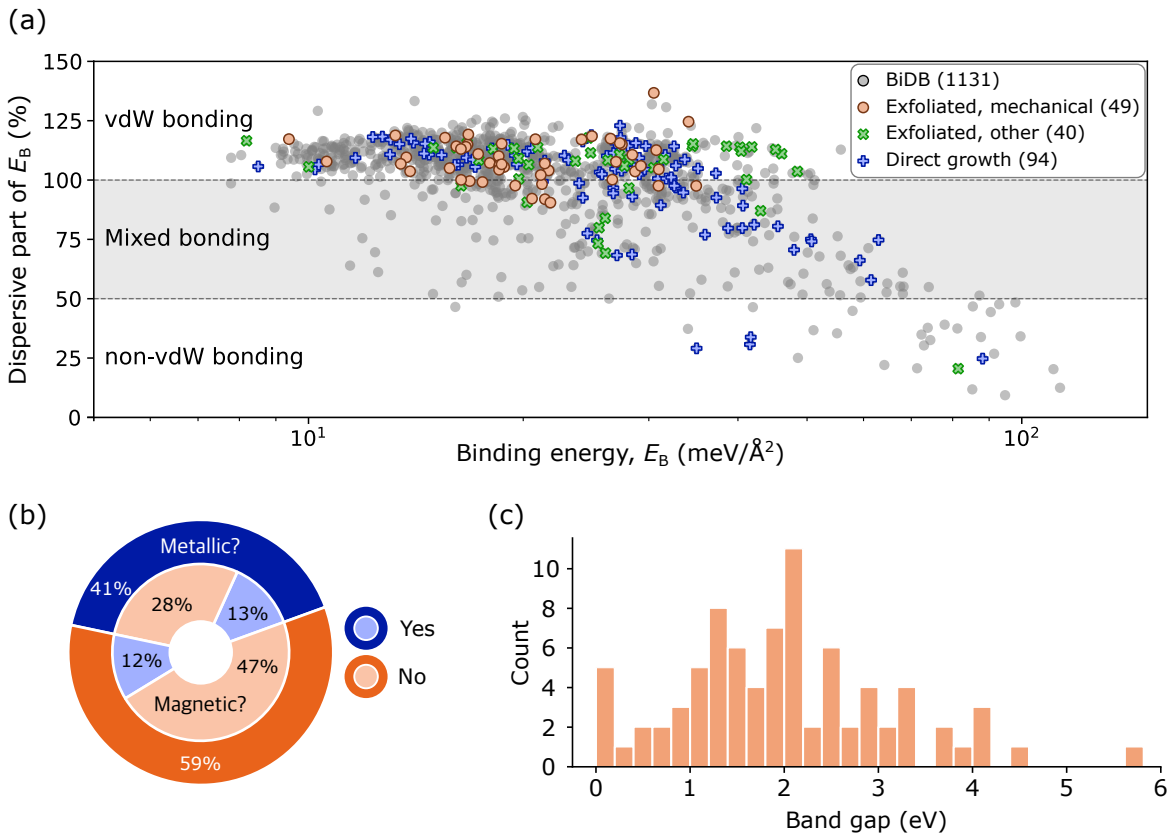


FIG. 5: **Computational Properties of Experimentally Realized 2D Materials.** All colored data refers to materials from X2DB that have been produced in few-layer form with thickness below 10 nm and have been linked to a monolayer in C2DB with high confidence level. (a) Interlayer binding energies calculated with the PBE-D3 method. The contribution of the dispersive D3-term to the binding energy is plotted as function of the total binding energy, E_B . Grey symbols show all materials in the computational bilayer database BiDB. Materials in X2DB are highlighted depending on whether they were mechanically exfoliated (orange), exfoliated by other techniques (green), or directly grown (blue). The type of interlayer bonding can be classified according to whether it is dominated by dispersive forces (vdW bonding), covalent or ionic bonding (non-vdW bonding), or a mixture of both (mixed bonding regime). (b) Distribution of the calculated electronic and magnetic properties of the monolayer form of the materials in X2DB. The outer ring shows the fraction of metallic vs. non-metallic monolayers. The inner ring shows the fraction of magnetic vs. non-magnetic materials further separated into metallic and non-metallic categories. (c) The band gap distribution for non-metallic materials, as calculated with the HSE06 xc-functional.

out-of-plane periodicity to be well defined and measurable. For very thin samples, in particular monolayers and bilayers, the concept is not even meaningful (see also the discussion in Sec. VI on space groups versus layer groups). All abbreviations used in Figure 4 are defined in Tables S1 and S2 in the SI.

V. INTEGRATION OF COMPUTATIONAL DATA

The integration of computational data with X2DB enables direct comparison between measured and calculated properties, as well as exploration of predicted properties beyond those accessible experimentally. Below we give a few illustrative examples.

Figure 5(a) shows the calculated exfoliation energy (more precisely the binding energy of the homobilayer in its most stable stacking configuration) plotted along the x -axis for all the materials in X2DB that have been matched with a monolayer in C2DB with high confidence level and have been realized with minimum thickness below 10 nm. The grey symbols represent all the homobilayers in the computational homobilayer database BiDB[46]. We note in passing that BiDB contains more than 3,000 homobilayers constructed by stacking 1000 of the most stable monolayers from C2DB in all possible lattice matched, i.e. non-moir, stacking configurations. In Figure 5(a), the materials from X2DB have been grouped according to synthesis method: Orange symbols denote materials with at least one entry in X2DB reporting synthesis by direct, i.e. non-assisted, mechanical exfolia-

tion (e.g. Scotch-tape method); green symbols represent materials with at least one entry reporting exfoliation by some other techniques (e.g. ultrasonication, electrochemical intercalation, or selective etching); blue symbols represent bottom-up grown materials (e.g. CVD, MBE). Note that the division is somewhat ambiguous as many materials can be produced by various methods. However, the results may still be used to explore limits for exfoliation. In particular, it is clear that except for a couple of outliers, all mechanically exfoliated materials have binding energy below $40 \text{ meV}/\text{\AA}^2$.

The binding energies in Figure 5(a) were calculated using the PBE-D3 functional, where the D3 correction adds an empirical description of long-range van der Waals (dispersion) forces that the standard PBE functional otherwise misses.[47] The values on the y -axis of Figure 5(a) show the relative contribution of the D3 term to the total interlayer binding energy. On this basis, three different bonding regimes can be identified: The vdW regime, where the PBE (i.e. non-vdW) contribution to the binding energy is negative due to Pauli repulsion. The non-vdW regime, where the PBE contribution to E_B dominates the dispersive D3 contribution, and the mixed bonding regime, where PBE contributes to the binding but does not exceed the D3 contribution.

While most of the mechanically exfoliated materials in Figure 5(a) fall within the vdW bonding region, several materials obtained with other exfoliation methods lie in the mixed bonding regime. The 2D electride Ca_2N is a notable outlier.[48] Located in the non-vdW region, Ca_2N exhibits a large binding energy of $80 \text{ meV}/\text{\AA}^2$, yet it has been exfoliated using ultrasonication. This unique behavior is attributed to electrostatic interactions between the $[\text{Ca}_2\text{N}]^+$ layers and the interstitial electron gas, which are fundamentally different from the weaker vdW forces governing bonding in the dispersive regime and the stronger and more directional covalent bonds. Among the directly grown 2D materials, several are located in the mixed and non-vdW bonding regions with binding energies reaching $90 \text{ meV}/\text{\AA}^2$.

Figure 5(b) shows an overview of the calculated electronic type (metallic or non-metallic) and magnetic state of the materials in X2DB. Only materials with a high C2DB confidence level are included. The results refer to the monolayer form of the materials. It can be seen from the outer ring of the diagram that 59% of the realized 2D materials are predicted by DFT to be semiconductors or insulators while 41% are predicted to be metals. The inner shell reveals that 25% of the materials are predicted to favor a magnetic over a non-magnetic ground state. Moreover, there is a relatively higher fraction of magnetic materials among the metals than among the non-metals.

We emphasize that the DFT calculations presented in Figure 5(b) do not capture strong electronic correlations, including possible Mott insulating states. Consequently, the computed fraction of metallic materials may be higher than what is observed experimentally. A recent

assessment of electronic and magnetic properties of more than 600 monolayer materials containing $3d$ transition metals, showed that introducing a Hubbard U -term in the DFT Hamiltonian, to improve the description of localized states, resulted a metal-to-insulator transition in 21% of the materials. In contrast, the magnetic ground state was largely unaffected by the U -term.[49]

Finally, Figure 5(c) shows the distribution of band gaps calculated with the HSE06 hybrid functional[50] for the non-metallic monolayers in X2DB. Again, only materials with a high C2DB confidence level are shown. The band gaps span from 0 to 5.7 eV (with hBN having the largest gap). In general, it is expected that bilayer and multilayer structures will have smaller band gaps than the monolayers (shown here), due to interlayer hybridization and increased dielectric screening – both of which tend to reduce the fundamental gap. On the other hand, the HSE06 functional typically underestimates fundamental band gaps compared to experiments and more accurate many-body methods. In fact, the HSE06 was found to underestimate the G_0W_0 band gap by around 20% for a set of 250 2D semiconductors[19].

VI. CLASSIFICATION OF 2D MATERIALS

To provide a systematic overview of all experimentally realized 2D materials, we have constructed a hierarchical classification based on the curated data in X2DB. The classification is listed in Table I and shown graphically in Fig. 6. The main classes are defined primarily by the anion type and comprise the historically important elemental 2D materials (Xenes), the chalcogenides, the halides, the oxides, the carbides and nitrides (including MXenes), and mixed-anion compounds. In Fig. 6 and Table I, the main classes are distinguished by color. Subclasses are mainly defined by chemical stoichiometry and/or cation group, and the final end-classes typically contain 310 members with similar chemical composition, structural type, and basic electronic/chemical properties.

Beyond providing a compact overview, this classification serves as an organisational backbone for the X2DB data. It enables comparison of trends within and across chemically related families (e.g. band gaps, stability, or magnetic order within a given anion class), highlights sparsely populated or entirely missing regions of 2D materials space, and thus points to promising directions for targeted synthesis. The hierarchy also defines natural “families” that can be used to construct balanced benchmark sets for machine-learning models, to design property-screening studies focused on specific application domains (such as catalysis or optoelectronics), and to consistently place newly reported 2D materials into the existing landscape.

The right column in Table I provides a brief summary of the main structural and electronic characteristics of the members of each class, including their typical crystal symmetry groups and main application area. We empha-

size that space groups (SGs) should be used exclusively to describe a bulk/multilayer form of a 2D material where the out-of-plane periodicity is well defined. In contrast, monolayer structures, which lack out-of-plane periodicity, are better described by their layer group (LG).[7] The same monolayer can be stacked in different ways to produce bulk or multilayer structures with different SGs. To avoid this ambiguity, we consistently use LGs for monolayers and SGs for bulk/multilayer structures.

VII. DISCUSSION

The open X2DB database with its curated, taxonomy-based data set and field-wide classification of experimentally realized 2D materials, provides a structured, global overview of the rich compound space that underpins the rapidly evolving field of 2D materials. Its tight integration of experimental and computational data enables seamless navigation between real-world measurements and theoretical predictions opening new opportunities to interrogate the factors governing stability and synthesizability, perform statistical inference across the literature, and guide the targeted discovery of novel 2D compounds. X2DB can also be used to identify holes in the current 2D materials map arising, for example, from biases in the choice of anions, metals, or synthesis strategies and to infer promising synthesis routes and growth substrates for specific compositions and material families.

At the time of writing, the X2DB contains 370 unique compounds, a number that is likely close to the full set of 2D materials that have been experimentally realized to date. Of these, 210 materials have been matched with high confidence to their monolayer, homobilayer, and bulk counterparts in mutually consistent first-principles databases. However, the purpose of X2DB extends far beyond serving as a showcase of previously synthesized 2D materials linked to computational data. By collecting multiple experimental records for the same compound, the database enables systematic exploration of how sample morphology and quality vary with synthesis approach, substrate, and related parameters, and it supports comprehensive overviews of the characterization techniques, measured physical properties, and reported applications for a given material of interest. Likewise, X2DB can be used to identify publications reporting specific types of measurements – such as Raman spectra, charge density waves, excitons, magnons, etc. – across different materials.

While experimental data sets can be contributed through a simple web form, only data related to published work can currently be registered. This requirement ensures the highest standards of reliability, traceability, and documentation of the data. Future developments may allow the inclusion of unpublished results, should the need arise.

The continued growth and usefulness of X2DB will rely

on active community engagement. By contributing their experimental data and publications, researchers not only increase the visibility and FAIRness of their work, but also enrich it by enabling links to complementary computational data. Beyond individual benefits, such data contributions are essential for advancing X2DB to a dynamic community resource that evolves continuously and provides lasting value to both experimentalists and theorists across the 2D materials field.

VIII. DATA AVAILABILITY

The open X2DB database is available at <https://x2db.fysik.dtu.dk/>.

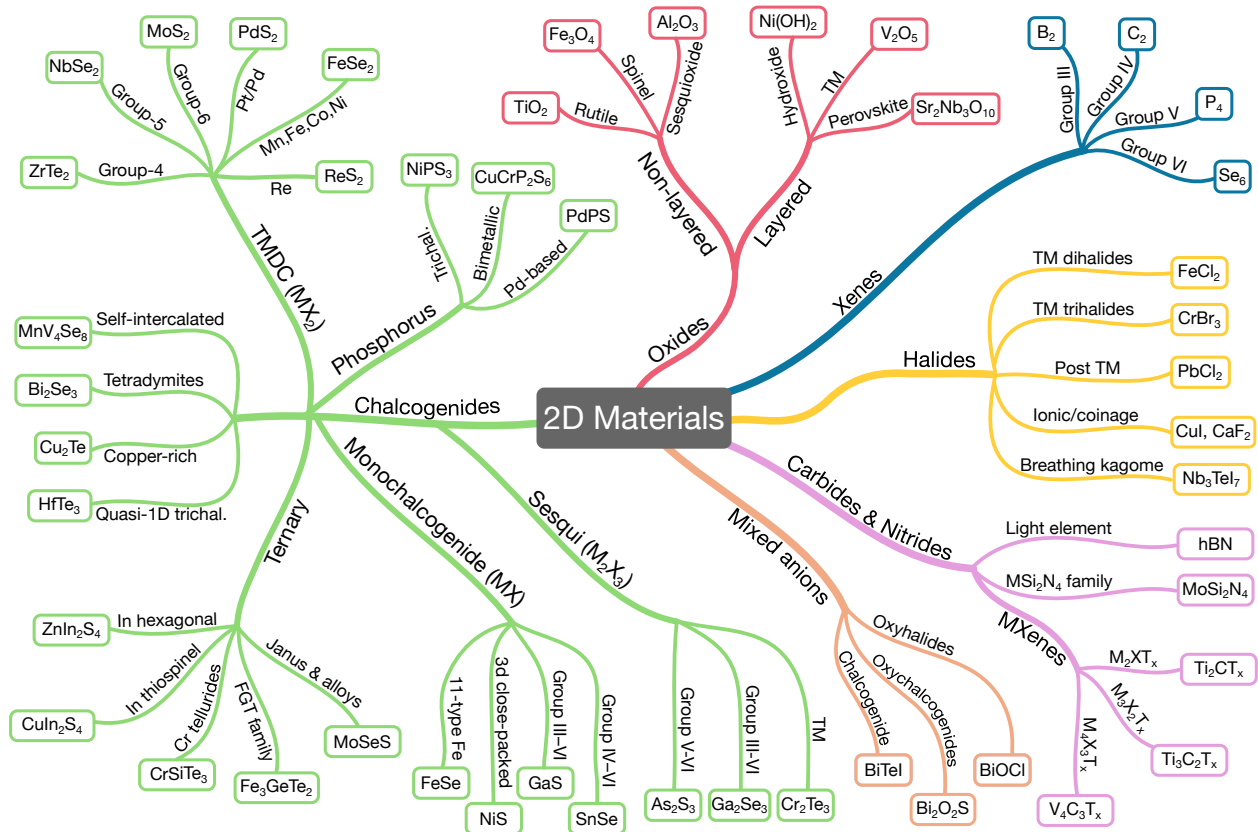


FIG. 6: **Hierarchical classification tree of experimentally realized 2D materials.** The main classes are distinguished by different colors (consistent with Table I) and branch out into subclasses and terminal classes. The hierarchy of classes is determined primarily according to anion-type, chemical composition/stoichiometry, and crystal structure, respectively. One representative member from each terminal class is shown at the end of the branches.

-
- [1] W. Ren, P. Boggild, J. M. Redwing, K. S. Novoselov, L. Sun, Y. Qi, K. Jia, Z. Liu, O. Burton, J. A. Alexander-Webber, *et al.*, *2D Materials* (2025).
- [2] L. He, H. Zhuang, Q. Fan, P. Yu, S. Wang, Y. Pang, K. Chen, and K. Liang, *Materials Horizons* **11**, 4239 (2024).
- [3] B. Anasori, M. R. Lukatskaya, and Y. Gogotsi, in *MXenes* (Jenny Stanford Publishing, 2023) pp. 677–722.
- [4] F. J. G. de Abajo, D. N. Basov, F. H. L. Koppens, L. Orsini, *et al.*, *ACS Photonics* **12**, 3961 (2025).
- [5] H. Song, J. Liu, B. Liu, J. Wu, H.-M. Cheng, and F. Kang, *Joule* **2**, 442 (2018).
- [6] X. Liu and M. C. Hersam, *Nature Reviews Materials* **4**, 669 (2019).
- [7] J. Fu, M. Kuisma, A. H. Larsen, K. Shinohara, A. Togo, and K. S. Thygesen, *2D Materials* **11**, 035009 (2024).
- [8] L. Song, L. Ci, H. Lu, P. B. Sorokin, C. Jin, J. Ni, A. G. Kvashnin, D. G. Kvashnin, J. Lou, B. I. Yakobson, and P. M. Ajayan, *Nano Letters* **10**, 3209 (2010).
- [9] L. Ma, C. Ye, Y. Yu, X. F. Lu, X. Niu, S. Kim, D. Feng, D. Tománek, Y.-W. Son, X. H. Chen, *et al.*, *Nature communications* **7**, 10956 (2016).
- [10] Q. H. Wang, K. Kalantar-Zadeh, A. Kis, J. N. Coleman, and M. S. Strano, *Nature Nanotechnology* **7**, 699 (2012).
- [11] K. S. Novoselov, A. K. Geim, S. V. Morozov, D. Jiang, Y. Zhang, S. V. Dubonos, I. V. Grigorieva, and A. A. Firsov, *Science* **306**, 666 (2004).
- [12] B. Zhao, D. Shen, Z. Zhang, P. Lu, M. Hossain, J. Li, B. Li, and X. Duan, *Advanced Functional Materials* **31**, 2105132 (2021).
- [13] H. Wang, X. Huang, J. Lin, J. Cui, Y. Chen, C. Zhu, F. Liu, Q. Zeng, J. Zhou, P. Yu, *et al.*, *Nature Communications* **8**, 394 (2017).
- [14] C. Wang, L. You, D. Cobden, and J. Wang, *Nature Materials* **22**, 542 (2023).
- [15] S.-Y. Xu, Q. Ma, H. Shen, V. Fatemi, S. Wu, T.-R. Chang, G. Chang, A. M. M. Valdivia, C.-K. Chan, Q. D. Gibson, *et al.*, *Nature Physics* **14**, 900 (2018).
- [16] M. Gibertini, M. Koperski, A. F. Morpurgo, and K. S. Novoselov, *Nature nanotechnology* **14**, 408 (2019).
- [17] D. Zagorac, H. Müller, S. Rühl, J. Zagorac, and S. Rehme, *Applied Crystallography* **52**, 918 (2019).
- [18] A. Jain, S. P. Ong, G. Hautier, W. Chen, W. D. Richards, S. Dacek, S. Cholia, D. Gunter, D. Skinner, G. Ceder, *et al.*, *APL Materials* **1** (2013).
- [19] S. Hastrup, M. Strange, M. Pandey, T. Deilmann, P. S. Schmidt, N. F. Hinsche, M. N. Gjerding, D. Torelli, P. M. Larsen, A. C. Riis-Jensen, J. Gath, K. W. Jacobsen, J. Jørgen Mortensen, T. Olsen, and K. S. Thygesen, *2D Materials* **5**, 042002 (2018).
- [20] D. Campi, N. Mounet, M. Gibertini, G. Pizzi, and N. Marzari, *ACS Nano* **17**, 11268 (2023).
- [21] J. Zhou, L. Shen, M. D. Costa, K. A. Persson, S. P. Ong, P. Huck, Y. Lu, X. Ma, Y. Chen, H. Tang, *et al.*, *Scientific Data* **6**, 86 (2019).
- [22] N. Mounet, M. Gibertini, P. Schwaller, D. Campi, A. Merkys, A. Marrazzo, T. Sohier, I. E. Castelli, A. Cepellotti, G. Pizzi, *et al.*, *Nature Nanotechnology* **13**, 246 (2018).
- [23] X. Wang, A. Chen, X. Wu, J. Zhang, J. Dong, and L. Zhang, *Nano-Micro Letters* **16**, 163 (2024).
- [24] M. Zhao, C. Casiraghi, and K. Parvez, *Chemical Society Reviews* **53**, 3036 (2024).
- [25] S. H. Choi, S. J. Yun, Y. S. Won, C. S. Oh, S. M. Kim, K. K. Kim, and Y. H. Lee, *Nature Communications* **13**, 1484 (2022).
- [26] B. Ryu, L. Wang, H. Pu, M. K. Y. Chan, and J. Chen, *Chemical Society Reviews* **51**, 1899 (2022).
- [27] S. Manti, M. K. Svendsen, N. R. Knøsgaard, P. M. Lynghby, and K. S. Thygesen, *NPJ computational materials* **9**, 33 (2023).
- [28] J. Björk, J. Zhou, P. O. Persson, and J. Rosen, *Science* **383**, 1210 (2024).
- [29] S. Americo, I. E. Castelli, and K. S. Thygesen, *ACS Electrochemistry* (2025).
- [30] Y.-C. Lin, R. Torsi, R. Younas, C. L. Hinkle, A. F. Rigosi, H. M. Hill, K. Zhang, S. Huang, C. E. Shuck, C. Chen, Y.-H. Lin, D. Maldonado-Lopez, J. L. Mendoza-Cortes, J. Ferrier, S. Kar, N. Nayir, S. Rajabpour, A. C. T. van Duin, X. Liu, D. Jariwala, J. Jiang, J. Shi, W. Mortelmans, R. Jaramillo, J. M. J. Lopes, R. Engel-Herbert, A. Trofe, T. Ignatova, S. H. Lee, Z. Mao, L. Damian, Y. Wang, M. A. Steves, K. L. Knappenberger, Z. Wang, S. Law, G. Bepete, D. Zhou, J.-X. Lin, M. S. Scheurer, J. Li, P. Wang, G. Yu, S. Wu, D. Akinwande, J. M. Redwing, M. Terrones, and J. A. Robinson, *ACS Nano* **17**, 9694 (2023).
- [31] X. Zhang, A. Chen, L. Chen, and Z. Zhou, *Advanced Energy Materials* **12**, 10.1002/aenm.202003841 (2022).
- [32] S. Lebègue, T. Björkman, M. Klintonberg, R. M. Nieminen, and O. Eriksson, *Physical Review X* **3**, 031002 (2013).
- [33] G. Cheon, K.-A. N. Duerloo, A. D. Sendek, C. Porter, Y. Chen, and E. J. Reed, *Nano Letters* **17**, 1915 (2017).
- [34] M. Ashton, J. Paul, S. B. Sinnott, and R. G. Hennig, *Physical Review Letters* **118**, 106101 (2017).
- [35] J. Feng, H. Gao, T. Li, X. Tan, P. Xu, M. Li, L. He, and D. Ma, *ACS Nano* **15**, 3415 (2021).
- [36] C. van Efferen, J. Hall, N. Atodiressei, V. Boix, A. Safeer, T. Wekking, N. A. Vinogradov, A. B. Preobrajenski, J. Knudsen, J. Fischer, *et al.*, *ACS Nano* **18**, 14161 (2024).
- [37] B. Feng, Z. Ding, S. Meng, Y. Yao, X. He, P. Cheng, L. Chen, and K. Wu, *Nano Letters* **12**, 3507 (2012).
- [38] X. Zhao, P. Song, C. Wang, A. C. Riis-Jensen, W. Fu, Y. Deng, D. Wan, L. Kang, S. Ning, J. Dan, *et al.*, *Nature* **581**, 171 (2020).
- [39] J. Karthikeyan, H.-P. Komsa, M. Batzill, and A. V. Krasheninnikov, *Nano Letters* **19**, 4581 (2019).
- [40] A. Raja, L. Waldecker, J. Zipfel, Y. Cho, S. Brem, J. D. Ziegler, M. Kulig, T. Taniguchi, K. Watanabe, E. Malic, *et al.*, *Nature nanotechnology* **14**, 832 (2019).
- [41] K. S. Thygesen, *2D Materials* **4**, 022004 (2017).
- [42] B. Radisavljevic and A. Kis, *Nature materials* **12**, 815 (2013).
- [43] S. Pakdel, A. Rasmussen, A. Taghizadeh, M. Kruse, T. Olsen, and K. S. Thygesen, *Nature Communications* **15**, 932 (2024).
- [44] J. H. Jung, C.-H. Park, and J. Ihm, *Nano letters* **18**, 2759 (2018).
- [45] J. J. Mortensen, A. H. Larsen, M. Kuisma, A. V. Ivanov, A. Taghizadeh, A. Peterson, A. Haldar, A. O. Dohn,

- C. Schäfer, E. Jónsson, E. D. Hermes, F. A. Nilsson, G. Kastlunger, G. Levi, H. Jónsson, H. Häkkinen, J. Fojt, J. Kangsabanik, J. Sødequist, J. Lehtomäki, J. Heske, J. Enkovaara, K. T. Winther, M. Dulak, M. M. Melander, M. Ovesen, M. Louhivuori, M. Walter, M. Gjerding, O. Lopez-Acevedo, P. Erhart, R. Warmbier, R. Würdemann, S. Kaappa, S. Latini, T. M. Boland, T. Bligaard, T. Skovhus, T. Susi, T. Maxson, T. Rossi, X. Chen, Y. L. A. Schmerwitz, J. Schiøtz, T. Olsen, K. W. Jacobsen, and K. S. Thygesen, *The Journal of Chemical Physics* **160**, 10.1063/5.0182685 (2024).
- [46] S. Pakdel, A. Rasmussen, A. Taghizadeh, M. Kruse, T. Olsen, and K. S. Thygesen, *Nature Communications* **15**, 932 (2024).
- [47] S. Grimme, S. Ehrlich, and L. Goerigk, *Journal of Computational Chemistry* **32**, 1456 (2011).
- [48] D. L. Druffel, K. L. Kuntz, A. H. Woomer, F. M. Alcorn, J. Hu, C. L. Donley, and S. C. Warren, *Journal of the American Chemical Society* **138**, 16089 (2016).
- [49] S. Pakdel, T. Olsen, and K. S. Thygesen, *npj Computational Materials* **11**, 18 (2025).
- [50] A. V. Krukau, O. A. Vydrov, A. F. Izmaylov, and G. E. Scuseria, *The Journal of Chemical Physics* **125** (2006).

TABLE I: **Hierarchical classification of experimentally synthesized 2D materials.** The table is organized into main classes (colored headings), subclasses (light-colored headings), and terminal classes, primarily according to anion-type, chemical composition/stoichiometry, and crystal structure, respectively. For each terminal class, representative examples from X2DB are listed. “X” in a chemical formula indicates that materials with all listed X-anion variants within the given subclass (e.g., X = S, Se, Te) are available in X2DB. The last column summarizes key features, with emphasis on crystal structure, electronic characteristics, and major application areas. A complete listing and primary references are provided in the Supplementary Information. Abbreviations: space group (SG) and layer group (LG).

Material class	Key characteristics
Members (not exhaustive)	
Monoelemental (Xenes)	
Group-III	
Borophene (B), Gallene (Ga)	Polymorphic (B) and honeycomb (Ga) structures. Substrate-stabilized and synthesis-sensitive. Metallic behaviour.
Group-IV	
Graphene (C), Silicene (Si), Germanene (Ge), Stanene (Sn), Plumbene (Pb)	Planar or low-buckled honeycomb atomic layers [LG 80 or 72]. Substrate-stabilized with no layered bulk form (except for graphene). Dirac-like band structures with spin-orbit coupling-driven gaps increasing from C \rightarrow Pb. Quantum spin Hall insulators.
Group-V	
Phosphorene (P), Arsenene (As), Antimonene (Sb), Bismuthene (Bi)	Exfoliable vdW-layered semiconductors [SG 166 or 64] consisting of buckled hexagonal [LG 72] (blue phosphorus) or puckered rectangular layers [LG 42] (black phosphorus); the latter with strong in-plane anisotropy. Band gaps shrink and the SOC increases from P \rightarrow Bi
Group-VI	
Selenene (Se), Tellurene (Te)	Nanosheets built from vdW-bonded helical Se or Te chains similar to those comprising the trigonal bulk phase [SG 152/154, depending on chain chirality]. The chain axis is typically within the 2D plane leading to in-plane anisotropic properties, but can be out-of-plane (isotropic). Semiconducting properties.
Chalcogenides	
Monochalcogenides (MX ; X = S, Se, Te)	
Group III–VI chalcogenides	
GaX, InSe	Exfoliable vdW-layered semiconductors with hexagonal X-M-M-X planes [LG 78 (X planes aligned) or 72 (X planes shifted)] and several stacking orders in bulk ($\beta, \epsilon, \gamma, \delta$) [SG 194,187,160,186]. Band gap from near-IR to UV. Strong nonlinear optics. High electron mobility.
Group IV–VI chalcogenides	
GeX, SnX, PbX	(Ge/Sn)(S/Se) are exfoliable vdW-layered semiconductors [SG 62] with puckered, orthorhombic layers [LG 32], strong in-plane anisotropy and ferroelectricity. PbX and SnTe are weakly distorted sheets of non-layered rocksalt [SG 225] with narrow band gap and strong spin-orbit coupling. High-performance thermoelectrics (thicker samples).
11-type Fe superconductors	
FeS, FeSe, FeTe	Layered tetragonal (PbO-type) structure [SG 129]. The monolayers are corrugated square nets of Fe with X below and above [LG 64]. FeS and FeSe are superconducting (low T _c); FeTe is metallic and anti-ferromagnetic.
3d hexagonal close-packed	
FeX, Fe ₇ S ₈ , NiS, CoTe, CrSe	Hexagonal close-packed NiAs-type structures (SG 194) built from hcp chalcogen layers with 3d metals in octahedral sites. Fe ₇ S ₈ is a vacancy-ordered NiAs-type. All members are metallic and many are magnetic. Note that the FeX members also adopt the tetragonal layered phase.
Transition metal dichalcogenides (TMDs) (MX₂ ; X = S, Se, Te)	
Group-4 TMDs	
TiX ₂ , ZrX ₂ , HfX ₂	Exfoliable vdW-layered crystals predominantly adopting a trigonal 1T polytype [SG 164] consisting of X-M-X monolayers with displaced X planes [LG 72]. (Zr/Hf)(S/Se) ₂ are indirect semiconductors. Remaining members are semimetals. TiSe ₂ exhibits charge density wave order.

Continued on next page

TABLE I: (continued)

Group-5 TMDs VX ₂ , NbX ₂ , TaX ₂	Exfoliable vdW-layered compounds crystallizing in the hexagonal 2H phase [SG 194] (most stable) or trigonal 1T phase [SG 164]. The constituent hexagonal X-M-X monolayers have the X planes aligned [LG 78] or shifted [LG 72], respectively. Correlated charge density wave metals. Superconductivity (NbS ₂ and NbSe ₂) and magnetism (VS ₂ and VSe ₂).
Group-6 TMDs CrX ₂ , MoX ₂ , WX ₂	Exfoliable vdW-layered crystals. The 2H polytype [SG 194; LG 78] is semiconducting with direct gap in monolayer and strong excitons. The polytypes 1T [SG 164; LG 72], 1T' [SG 11; LG 15] and Td [SG 31; LG 15] (the latter two are distorted 1T), are (semi)metallic or small gap-semiconductors. For few-layer Mo or W-based TMDs, a polymorphic 2H↔1T/1T' conversion can be driven by doping/intercalation/strain. Cr compounds in the 1T phase are metallic ferromagnets.
Pt/Pd TMDs PdX ₂ , PtX ₂	Exfoliable vdW-layered crystals. PtX ₂ and PdTe ₂ adopt the 1T polytype [SG 164; LG 72] while PdS ₂ and PdSe ₂ adopt an orthorhombic structure [SG 61] with one-atom thick slightly buckled "pentagonal" layers [LG 17]. Generally, strong interlayer coupling that drives a transition from semiconductor (monolayer) to semimetal/narrow gap (few-layer). Bulk PdTe ₂ is a Dirac semimetal and superconducting.
(Mn,Fe,Co,Ni)-TMDs MnX ₂ , FeX ₂ , CoX ₂ , NiX ₂	Generally non-layered bulk forms (except NiTe ₂ [SG 164]). Directly grown 2D layers can adopt 1T/1T' or pyrite/marcasite-derived non-vdW polymorphs. Electronic properties varies depending on composition and polytype.
Re TMDs ReS ₂ , ReSe ₂	Exfoliable vdW-layered semiconductors [SG 2]. The monolayers have a 2×2-distorted 1T structure (1T'') [LG 2]. Strong in-plane anisotropy and weak thickness dependence of band gap (i.e. weak interlayer coupling)
Sesqui-chalcogenides (M₂X₃; X = S, Se, Te)	
Transition metals Cr ₂ X ₃ , Co ₂ Te ₃ , Nb ₂ S ₃	Non-vdW layered NiAs-derived structures consisting of close-packed chalcogen layers with cations in octahedral sites with ordered vacancies [SG 194,148,163]. Directly grown atomically thin samples adopt similar motifs, and can be often be viewed as M-intercalated 1T-MX ₂ structures. Magnetism is common in the Cr/Co members.
Group III-VI Ga ₂ S ₃ , Ga ₂ Se ₃ , In ₂ X ₃	Predominantly non-vdW and polymorphic. Vacancy-ordered frameworks (defect zinc blende or wurtzite derivatives) are common. The exception is the vdW-layered In ₂ Se ₃ with many polymorphs [e.g. SG 160, 166, 186] built from one of two quintuple Se-In-Se-In-Se monolayer types [LG 72,69]. Main application in optoelectronics (photodetectors, nonlinear optics).
Group V-VI As ₂ S ₃ , As ₂ Se ₃ , Sb ₂ S ₃ , Sb ₂ Se ₃ , Bi ₂ S ₃	Exfoliable vdW semiconductors consisting of quasi-1D structures (Sb-based and Bi ₂ S ₃) [SG 62] or monoclinic, corrugated sheets with strong in-plane anisotropy (As-based) [SG 14; LG 32]. The As structures are in-plane ferroelectricity.
Ternary chalcogenides (X = S, Se, Te)	
MX₂ Janus and alloys WSSe, MoSSe, NbSSe, CrSSe, TiSSe	Janus monolayers, such as MoSSe, WSSe, NbSSe, consist of X-M-Y atomic planes with different chalcogens on opposite sides of the metal layer giving rise to a permanent out-of-plane polarization [LG 69]. In contrast, alloys have randomly distributed S and Se [LG 72/78 for 1T/2H phases] and concentration-dependent properties such as tunable excitons.

Continued on next page

TABLE I: (continued)

FGT family Fe_3GeTe_2 , Ni_3GeTe_2 , Fe_3GaTe_2 , Fe_4GeTe_2 , Fe_5GeTe_2	Exfoliable vdW-layered metallic ferromagnets built from Te-terminated hexagonal slabs with Fe–Ge(Ga)–Fe blocks. The base structures Fe_3XTe_2 have the same layer group as the 2H-TMD structure and lacks inversion symmetry [LG 72]. Thickness-dependent magnetism. Fe_5 and Ga compounds have Curie temperatures close to room temperature. Applications in spintronics and electrocatalysis.
Cr-based tellurides CrSiTe_3 , CrGeTe_3	Exfoliable vdW-layered materials [SG 148]. The monolayer consists of a honeycomb lattice of octahedrally coordinated Cr atoms with upright Si or Ge dimers in the hexagon centers [LG 71]. Small gap semiconductors, which exhibit ferromagnetic order and large spin-orbit effects. Evidence for strong spin-lattice coupling.
In-based thiospinels (MIn_2S_4) CuIn_2S_4 , CaIn_2S_4 , MgIn_2S_4 , MnIn_2S_4	Non-layered cubic spinel-type structures [SG 227]. Ultrathin nanosheets can be synthesized using e.g. hydrothermal methods. Applications in (photo)catalysis and battery electrodes.
In-based layered hexagonal (MIn_2X_4) ZnIn_2S_4 , FeIn_2S_4 , MnIn_2Se_4	Layered spinel-family semiconductors built from hexagonal seven-atom-thick monolayers of the form X-(M/In)-X-(In/M)-X-In-X [LG 72,69]. Different stackings of one of these monolayers lead to many layered polytypes [e.g. SG 160,166,186,156]. Many compositions also exhibit non-vdW cubic spinel-type polymorphs [SG 227]. Relatively small and thickness-dependent band gap. Possible magnetism for Mn/Fe members.
Phosphorus chalcogenides	
Phosphorus trichalcogenides (MPX_3) MnPX_3 , FePX_3 , CdPX_3 , CoPS_3 , NiPS_3	Exfoliable vdW layered semiconductors. Structure similar to the MX_3 trihalides (e.g. CrI_3) with a honeycomb lattice of transition metal atoms. Many compounds are magnetic with varying types of anti-ferromagnetic order. For example, zigzag order with in-plane (Ni), out-of-plane (Fe) easy axis or in-plane Néel order (Mn). The corresponding Cr compound is more stable as CrPS_4 - a vdW layered monoclinic structure that exhibits ferromagnetic order within the layers.
Bimetallic phosphochalcogenides CuCrP_2S_6 , CuInP_2S_6 , CuVP_2S_6 , $\text{AgInP}_2\text{Se}_6$	Exfoliable vdW layered compounds with monolayers built from $[\text{P}_2\text{X}_6]^{4-}$ units with two distinct metal sublattices ($A = \text{Cu/Ag}$, $B = \text{Cr, V, In}$). Semiconductors with band gaps in the range 1-3 eV and out-of-plane ferroelectricity arising from off-centering of the Cu/Ag ions.
Pd-based phosphochalcogenides $\text{Pd}_3\text{P}_2\text{S}_8$, PdPS , PdPSe	Exfoliable vdW layered semiconductors. The monolayers of $\text{Pd}_3\text{P}_2\text{S}_8$ consist of a planar Pd kagome lattice augmented by up/down-alternating $[\text{PS}_4]^{3-}$ ions situated at the Pd triangles. PdPX ($X=\text{S,Se}$) consist of double-atom puckered pentagonal layers and exhibit strong in-plane anisotropic and nonlinear optical response.
Other chalcogenides	
(Self-)intercalated TMDs MnV_4Se_8 , CrV_4Se_8 , Cr_2Se_3 , Cr_3Se_4 , Fe_3Se_4 , Ni_3Te_4 , V_9S_{16} , Ta_9S_{16} , V_7S_{12}	TMD-derived structures composed of stacked MX_2 layers with native or extrinsic metal atoms periodically intercalated in the vdW gaps. Typically metallic. Some compounds exhibit magnetism that depends on the intercalant species and concentration.
Tetradymites Bi_2Se_3 , Bi_2Te_3 , Bi_2TeSe_2 , MnBi_2Te_4	Note: For a given intercalation (ic) concentration, the stoichiometry differs between an isolated ic-bilayer and the ic-bulk material.
Tetradymites Bi_2Se_3 , Bi_2Te_3 , Bi_2TeSe_2 , MnBi_2Te_4	Exfoliable vdW compounds built from Bi–chalcogen quintuple or Mn-containing septuple slabs stacked along the hexagonal axis. Bi_2TeSe_2 has been realized both with the Te layer in the center and at the slab surface (Janus material with broken mirror symmetry). Narrow band gaps, strong spin-orbit coupling, non-trivial topology; intrinsic magnetism in MnBi_2Te_4 .

Continued on next page

TABLE I: (continued)

Cu-rich chalcogenides Cu ₂ S, Cu ₂ Se, Cu ₂ Te	Non-vdW compounds featuring close-packed chalcogen frameworks with Cu on (often partially occupied) interstitial sites. Strongly polymorphic, with temperature- and composition-driven structural phase transitions (including superionic phases). Narrow-gap, often degenerate <i>p</i> -type semiconductors. Directly grown ultrathin nanosheets can be viewed as a few Cu planes sandwiched between close-packed chalcogen layers derived from the bulk frameworks.
Quasi-1D trichalcogenides TiS ₃ , HfTe ₃ , ZrS ₃ , ZrSe ₃	Exfoliable quasi-1D layered semiconductors [SG 11]. The monolayers are chain-like structures with edge-sharing MX ₆ prisms forming ribbons packed into corrugated layers [LG 46]. The crystals cleave anisotropically into ribbon-like flakes. Strongly in-plane anisotropic transport and optical properties.
Halides	
Transition metal dihalides FeCl ₂ , FeBr ₂ , MnI ₂ , NiCl ₂ , NiBr ₂ , NiI ₂ , VCl ₂ , VBr ₂ , VI ₂	Exfoliable vdW-layered crystals built from X-M-X layers with the metal octahedrally coordinated between two hexagonal halogen sheets [LG 72]. The stacking order can be 1T or 3R [SG 164 or 166]. All are strongly correlated, magnetic and typically exhibits non-collinear or spiral order due to geometric frustration. The spiral structures implies type II multiferroic order and odd-parity magnetism.
Transition metal trihalides CrX ₃ , FeCl ₃ , RuCl ₃	Exfoliable vdW-layered semiconductors/insulators. The X-M-X layers consists of edge-sharing MX ₆ octahedra, where the transition-metal atoms form a 2D honeycomb lattice sandwiched between two nearly close-packed halide sheets [LG 71]. In bulk, the layers adopt 3R or monoclinically distorted 3R stacking [SG 148 or 12]. All CrX ₃ monolayers are ferromagnetic; CrCl ₃ has anti-ferromagnetic interlayer coupling. RuCl ₃ has been scrutinized for quantum spin liquid physics, but becomes anti-ferromagnetic at low temperatures.
Post transition metal halides PbCl ₂ , PbI ₂ , PbBr ₂ , CdI ₂ , HgI ₂ , BiI ₃ , BiBr ₃ , SbI ₃	vdW-bonded semiconductors/insulators. CdI ₂ and PbI ₂ adopt the layered hexagonal 1T structure [SG 164; LG 72]. SbI ₃ and BiI ₃ adopt the layered hexagonal CrI ₃ -type structure [SG 148; LG 71]. The remaining (listed) members crystallize in more complex molecular or quasi-1D frameworks.
Ionic and coinage halide salts CuI, CuBr, AgI, CaCl ₂ , CaF ₂	Crystallize as three-dimensional, non-vdW salts in bulk, often with multiple temperature- or pressure-driven polymorphs. Ultrathin 2D forms require bottom-up growth often with templating. Medium- to wide-gap insulators.
Breathing kagome lattices Nb ₃ Cl ₈ , Nb ₃ Br ₈ , Nb ₃ I ₈ , Nb ₃ TeI ₇	Exfoliable vdW-layered compounds [SG 164, 166, 186], all built from distorted ("breathing") kagome lattices of Nb atoms (Nb ₃ clusters) [LG 69]. Distortions breaks inversion symmetry resulting in (out-of-plane) polar structures. Prototypical one-band Mott-Hubbard insulators. Bulk forms are non-magnetic due to bilayer dimerization, but it is possible that magnetic order persists in the monolayer limit.
Oxides	
Layered	
Transition-metal oxides V ₂ O ₅ , MoO ₃ , WO ₃	Both V ₂ O ₅ [SG 59; LG 46] and MoO ₃ [SG 62; LG 15] are vdW-layered and directly exfoliable with strongly in-plane anisotropic structures. In contrast, bulk WO ₃ [SG 14] is a 3D framework of corner-sharing WO ₆ octahedra [SG 14]; few-layer WO ₃ nanosheets obtained via chemical conversion from layered chalcogenide precursors. Band gaps around 2-3 eV. Main applications in (photo)electrochemistry and catalysis.

Continued on next page

TABLE I: (continued)

Brucite-type hydroxides Ni(OH) ₂ , Co(OH) ₂ , Mg(OH) ₂ , Cd(OH) ₂	Brucite-like layered crystal structure [SG 164]. Monolayers adopt the hexagonal CdI ₂ -type motif [LG 72] and are held together predominantly by ionic and hydrogen bonding rather than vdW forces. Mg/Cd-based hydroxides are wide-gap band insulators/dielectrics while Ni/Co-based hydroxides are correlated, magnetic insulators. Mostly considered energy storage and (electro)catalysis applications.
Perovskite-like (A₂B₃O₁₀) Sr ₂ Nb ₃ O ₁₀ , Ca ₂ Nb ₃ O ₁₀ , Pb ₂ Nb ₃ O ₁₀	Perovskite slabs consisting of three layers of corner-shared BO ₆ octahedra with A cations filling the interstitial sites. Typically obtained by chemical exfoliation of layered Dion–Jacobsen bulk parents A'A ₂ B ₃ O ₁₀ (A' monovalent cation). Applications in ferroelectrics, dielectrics, and photodetectors.
Non-layered	
Stoichiometry note	Note that for non-layered compounds, the precise stoichiometry of a 2D nanosheet may differ from that of the bulk.
Rutile-type TiO ₂ , SnO ₂ , IrO ₂ , RuO ₂ , VO ₂ , WO ₂ , MoO ₂	Non-layered rutile or distorted rutile structures. Nanosheets with thickness down to a few unit cells, are typically obtained by thin-film deposition or solution-based soft-chemistry methods. Electronic properties vary. Main application in battery electrodes, photo/electrocatalysis, and sensing.
Sesquioxides Al ₂ O ₃ , Ga ₂ O ₃ , Fe ₂ O ₃ , Cr ₂ O ₃ , Bi ₂ O ₃ , Gd ₂ O ₃	Non-layered corundum-type (Al,Fe,Cr) and other dense sesquioxide structures. Wide-band gap semiconductors or insulators. Nanosheets with thickness down to a few unit cells are typically obtained by thin-film deposition or solution-based soft-chemistry methods.
Spinel-type Co ₃ O ₄ , Mn ₃ O ₄ , Fe ₃ O ₄	Non-layered spinel or spinel-related structures. Nanosheets with thickness down to a few unit cells are typically obtained by thin-film deposition or solution-based soft-chemistry methods. Applications within catalysis and electrochemistry.
Carbides and Nitrides	
Light-element nitrides/carbons h–BN, C ₃ N, CH	Covalent sp ² /sp ³ bonded honeycomb layers of light elements (B, C, N, H). Hexagonal BN is a vdW-layered insulator (SG 194; LG 78) widely used for encapsulation and protection of other 2D materials. Hydrogenated graphene (graphane, CH; LG 72) and graphene-derived semiconducting C ₃ N (e.g. LG 80) are typically realized as monolayers or few-layer films grown on substrates and do not have established vdW-layered bulk crystal phases.
MSi₂N₄- family MoSi ₂ N ₄ , WSi ₂ N ₄	Monolayers consist of septuple hexagonal atomic planes N-Si-N-Mo-N-Si-N [LG 78] with the central MN ₂ layer adopting the 2H-MoS ₂ -type motif. Although no bulk parent is known, direct synthesis yields layer by layer growth with clear vdW gaps between the layers. Semiconductors with high mechanical strength and ambient stability.
MXenes (M_{n+1}X_nT_x; X = N, C; T = -O, -F, -OH, -Cl, +more)	
MXenes general (all n)	Hexagonal metal layers with C/N in the interstitial octahedral sites. Typically produced by selective etching of a bulk MAX phase (A = Al, Ga, Si, ...) [SG 194] and subsequent delamination. The outer metal planes are terminated by, often mixed, surface groups T _x . Metallic or highly conductive with large accessible surface area. Surface chemistry largely governed by T _x . Widely explored for ion intercalation and pseudocapacitive energy storage (batteries, supercapacitors), electrochemical sensing and nonlinear optics.
M₂XT_x Ti ₂ CT _x , Ta ₂ CT _x , Zr ₂ CCl ₂ , Zr ₂ CBr ₂ , Ti ₂ NCl ₂	Surface terminated M–X–M trilayers [LG 72]. Structurally the simplest MXene members.

Continued on next page

TABLE I: (continued)

$M_3X_2T_x$ $Ti_3C_2T_x, Ti_3N_2T_x$	Surface terminated M–X–M–X–M (five atomic layers) [LG 72]. Include $Ti_3C_2T_x$, the prototypical and most widely studied MXene.
$M_4X_3T_x$ $Ti_4N_3T_x, V_4C_3T_x, Nb_4C_3T_x, Ta_4C_3T_x$	Surface terminated M–X–M–X–M–X–M slabs (seven atomic layers) [LG 72]. Thicker slabs provide enhanced mechanical robustness.
Mixed anions	
Oxychalcogenides $Bi_2O_2S, Bi_2O_2Se, Bi_2O_2Te$	Layered semiconductors built from $[Bi_2O_2]^{2+}$ layers alternating with X^{-2} chalcogenide layers. Bi_2O_2Se and Bi_2O_2Te [tetragonal, SG 139] are directly exfoliable while few-layer forms of Bi_2O_2S [orthorhombic, SG 58] have been obtained via solution chemistry. The band gaps decrease and SOC increase from S→Se→Te. These materials combine high electron mobility with attractive optoelectronic and nonlinear optical properties.
Chalcohalides $CrSBr, BiTeI$	Exfoliable vdW layered semiconductors. $CrSBr$ [SG 59] shows strong in-plane anisotropy; each layer forms a buckled rectangular body-centered lattice of Cr atoms [LG 46]) with ferromagnetic layers coupled anti-ferromagnetically along the stacking direction. $BiTeI$ consists of polar Janus 1T-MX ₂ -type trilayers with strong spin-orbit coupling and large Rashba effects.
Oxyhalides $BiOCl, GdOCl, LaOBr, NbOCl_2, NbOI_2$	Layered structures with $[M_2O_2]$ slabs; strong optical anisotropy and photocatalytic activity; emerging ferroelectricity in $NbOI_2$.

